Proceedings of Global Power and Propulsion Society
ISSN-Nr: 2504-4400
GPPS Hong Kong 2023
October 17-19, 2023
www.gpps.global

GPPS-TC-2023-245

DECARBONISATION OF HIGH-TEMPERATURE ENDOTHERMIC CHEMICAL REACTION PROCESSES USING A NOVEL TURBOMACHINE: ROBUSTNESS OF THE CONCEPT TO FEED VARIABILITY

Dylan Rubini
University of Oxford
dylan.rubini@eng.ox.ac.uk
Oxford, UK

Nikolas Karefyllidis
University of Oxford
nikolas.karefyllidis@eng.ox.ac.uk
Oxford, UK

Budimir Rosic
University of Oxford
budimir.rosic@eng.ox.ac.uk
Oxford, UK

Liping Xu
University of Cambridge
lpx1@cam.ac.uk
Cambridge, UK

Elina Nauha
Coolbrook Oy
elina@coolbrook.com
Helsinki, Finland

ABSTRACT

This paper presents a revolutionary turbomachinery concept, referred to as the turbo-reactor, which has the potential to replace gas-fired radiant furnaces and decarbonise a wide range of hard-to-abate, high-temperature endothermic chemical reaction processes. While previous studies by the authors have confirmed the feasibility of using a turbo-reactor for steam cracking reactions, the numerical investigation presented in this work demonstrates its potential for eliminating emissions from a variety of energy-intensive chemical processes, including those used in the hydrogen industry. This step change in technology could be the catalyst needed to enable rapid scale-up of low-carbon hydrogen technology. The innovative design of the turbo-reactor is fundamentally based on converting all the mechanical energy imparted into internal energy, rather than pressure. This enables temperatures of up to 1700 °C (depending on fluid properties) to be achieved within an axial length in the order of one metre, resulting in a 100 – 1000× increase in power density compared to a surface heat exchanger. This paper presents the first comprehensive analysis of the turbo-reactor's robustness and controllability across a broad spectrum of feeds, chemical reaction stages, Mach number regimes, and operating points, conclusively demonstrating the feasibility of a universal stage design strategy for various endothermic reaction processes.

INTRODUCTION

Motivation and Background

Decarbonisation of hard-to-abate high-temperature endothermic chemical reaction processes, such as steam cracking of hydrocarbons, ethylene dichloride cracking, plastic recycling, hydrogen production through steam methane reformation (SMR), and ammonia decomposition, is a significant challenge in this decade (Thiel and Stark, 2021). These chemical processes are essential components of large-scale, global industries. For instance, the hydrocarbon cracking market is presently valued at $240 billion, with a global annual capacity of 400 million tons per annum (Mtpa) (Bender, 2014). This is expected to grow to $350 billion, with a capacity of 600 Mtpa, by 2030. Additionally, with rapidly growing support for low-carbon hydrogen and ammonia for transport, industry, buildings, and power generation, their demand is set to increase exponentially over the next 30 years, potentially doubling to 200 Mtpa by 2030, with a market value of $320 billion (IEA, 2022).

Large-scale energy-intensive sectors (*e.g.,* chemical/petrochemicals, steel, and cement) account for almost 20% of global CO_2 emissions (IEA, 2021), primarily due to heat generated by fossil fuel combustion. To address this challenge, a new class of turbomachines has been developed to replace the gas-fired surface heat exchangers (specifically, the fire-box/furnace unit) used in these heavy industrial processes, as shown in Figure 1.

Heavy industry can be transformed radically by exploiting the complex flow physics and controllable energy conversion processes possible within a turbomachine. This novel turbomachine, known as the RotoDynamic Reactor (RDR) or turbo-reactor, works on the principle of directly imparting mechanical energy to the working fluid supplied by a renewably powered

electric motor as the mechanical driver (Rubini et al., 2021; Coolbrook Oy, 2022), as shown in Fig. 2(*a*). As a result, Fig. 1 demonstrates that the turbo-reactor can significantly increase power density by up to two orders of magnitude in comparison to a surface heat exchanger, leading to a reduced plant footprint, as well as lower capital, operating, and maintenance costs. This is achieved by converting almost all of the mechanical energy imparted into internal energy (see Fig. 2(*a*)), rather than compressing the gas as done in a compressor (which is another example of an energy-imparting machine). Therefore, high working fluid temperatures of up to 1700 °C can be achieved within short axial distances of less than one metre, depending on the working fluid properties. This can result in a significant improvement in the efficiency and yield of the reaction (Rubini et al., 2022*a*). Previous work by the authors presents a detailed introduction and analysis of stage design, energy transformation train, and fundamental flow physics (Rubini et al., 2021, 2022*a*,*b*; Karefyllidis et al., 2023).

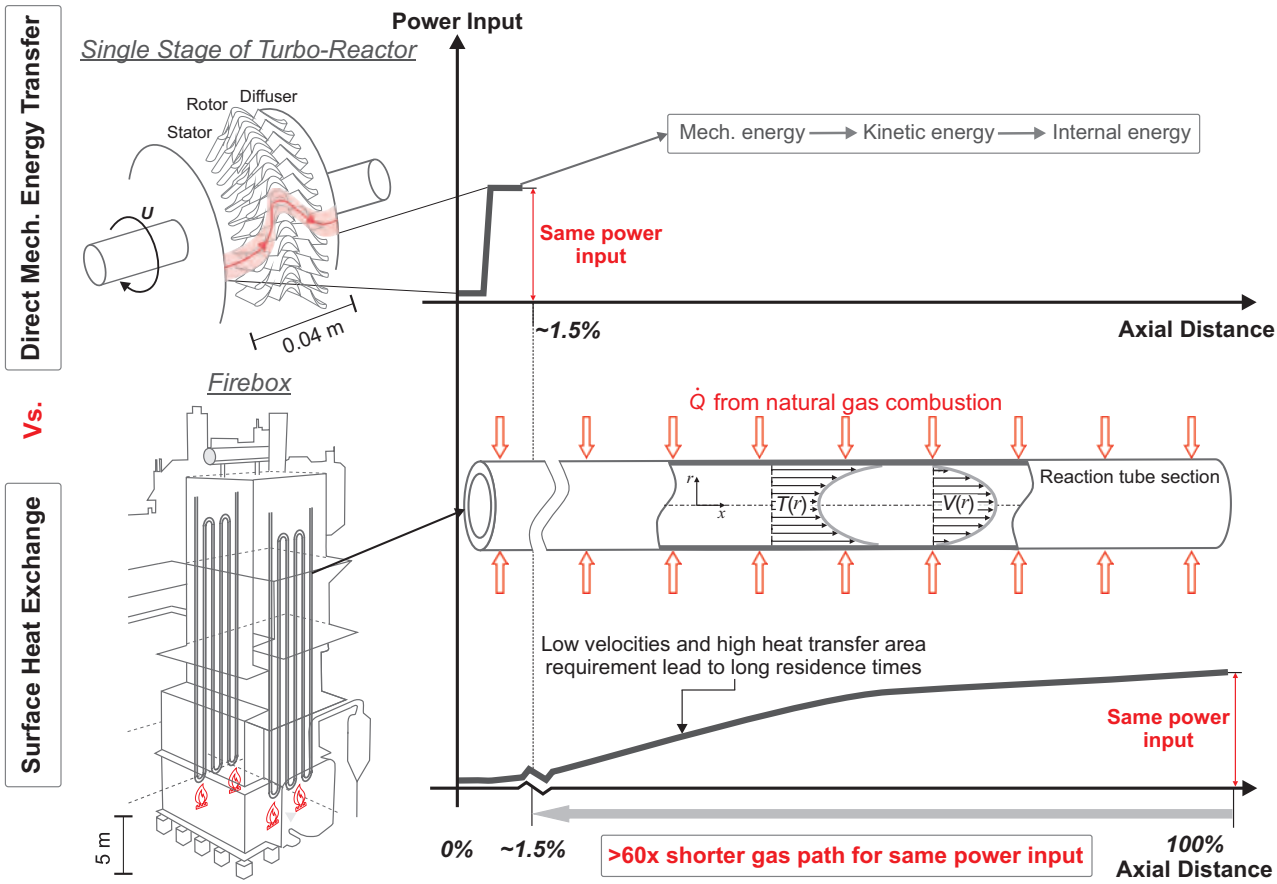

Figure 1 A schematic analysis of the energy transfer mechanism in a surface heat exchanger against that in the turbo-reactor

Figures 3 & 4 highlight the significant role of the RDR in decarbonising a diverse set of high temperature endothermic reaction processes for the production of high-value commodity chemicals in the chemical industry, such as steam cracking, thermochemical plastic waste recycling, SMR for hydrogen production, and ammonia decomposition for hydrogen recovery. Alternative strategies to decarbonise these sectors include hydrogen-fired (Weydahl et al., 2013) or electrified furnaces (Delikonstantis et al., 2019), but these suffer from large thermal resistances that hinder energy transfer (Venkataraman et al., 2003), low power density, and nonuniform temperature profiles within the reaction tubes, all of which can degrade process quality. Moreover, there are additional challenges related to scalability at high temperatures for electric furnaces and low energy conversion efficiency $\leq 60\%$ (Lu et al., 2022) and nitrous oxide emissions for hydrogen-fired furnaces.

Objectives of this Study

This first-of-its-kind paper demonstrates the applicability of the RDR for decarbonising a wide range of high-temperature endothermic reactions within the chemical industry (see Fig. 4). This study confirms the robustness and controllability of the system subjected to different feedstocks, variable chemical reaction states, and a range of operating points. A broad spectrum of operating states is generated by harnessing the variations of thermophysical/thermochemical fluid properties corresponding to different feedstocks (*e.g.,* n-hexane, methane, ammonia, etc.) and reaction progress states. The RDR is shown to be resilient, flexible, and free of system instability despite using a single machine with fixed boundary conditions.

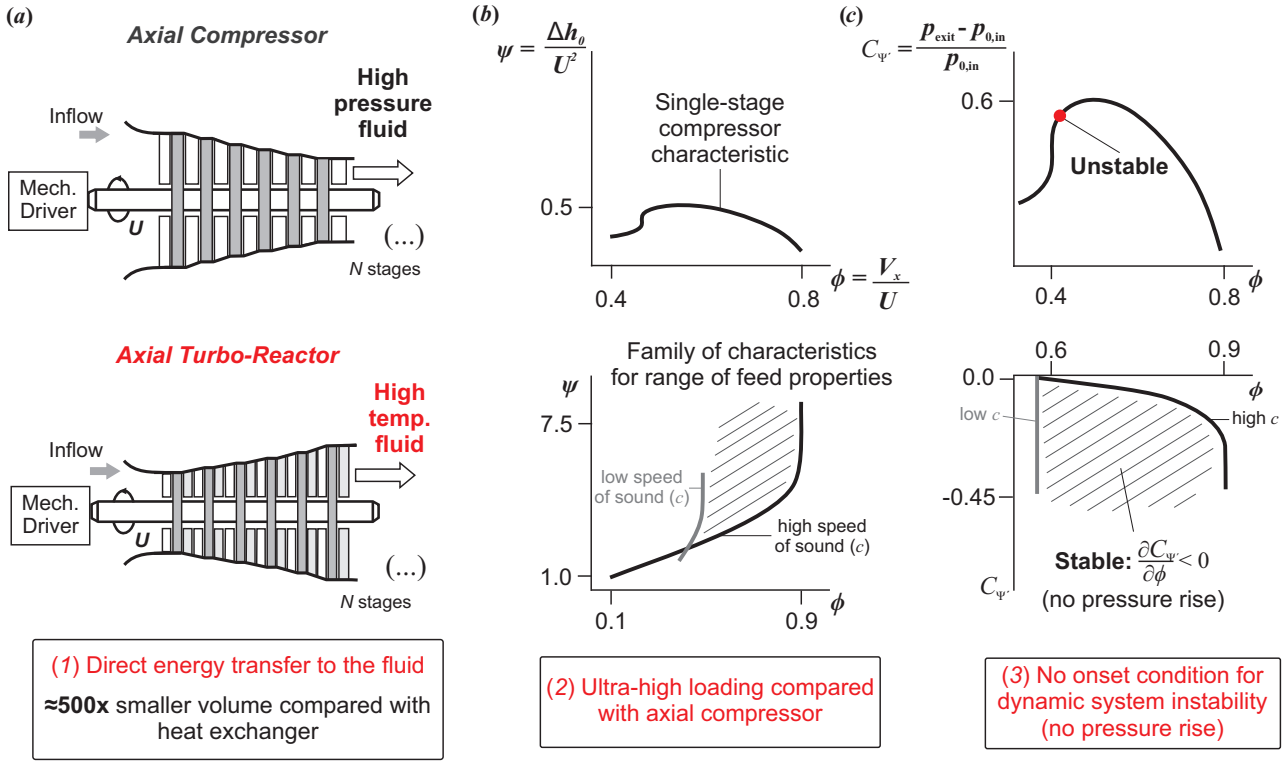

Figure 2 A comparison between an axial compressor and turbo-reactor (both energy imparting machines), showing (*a*) the primary objectives, (*b*) the single-stage flow coefficient ϕ against stage loading ψ characteristic speedline, and (*c*) the single-stage flow coefficient ϕ against total-to-static pressure rise coefficient $C_{\Psi'}$ characteristic speedline

THE TURBO-REACTOR: DIRECT ENERGY TRANSFER FOR ENDOTHERMIC CHEMICAL REACTIONS

Controllable Elemental Stage Design for Ultra-high Power Density Energy-Input

The turbo-reactor concept and detailed design have been developed over many years of collaboration with Coolbrook Oy (2022) and are based on the original patents by Bushuev (2016). This new machine unlocks a radically new design space for high-power-density energy-imparting machines, as shown in Figs. 2 & 3. Figure 2 compares the constant speed ϕ–ψ and ϕ–$C_{\Psi'}$ characteristics between the turbo-reactor and an axial compressor. As the primary objective for an axial compressor is pressure rise, the work coefficient ψ is limited by isentropic efficiency constraints over the entire operating range (see Fig. 2(*b*)), and system instability considerations at low flow coefficients ϕ (see Fig. 2(*c*)). By eliminating the requirement for a static pressure increase in the RDR, these constraints are bypassed within the relevant operating range (that is, $p_{\text{exit}}/p_{0,\text{in}} \leq 1$). This results in the following key design differences from a compressor:

1. For low molecular weight fluids, an ultra-high loading coefficient up to 7.5 is possible (see Fig. 2(*b*)). This is an order of magnitude higher than a typical axial compressor, minimising the number of stages required for heating. Figure 2(*b*) indicates that the work coefficient approximately linearly increases with the flow coefficient, before turning towards the vertical due to feed-composition-dependent choking limitations.

2. Within the choking limits of the working fluid, the RDR can achieve very high relative Mach numbers ($M_{\text{rel,max}} \approx 2.3$) and flow coefficients (up to $\phi \approx 0.9$) without the risk of system instability and overall performance degradation. This enables a high flow capacity per unit frontal area, resulting in a smaller machine footprint.

3. Since there is no requirement to support a global adverse pressure gradient, Fig. 2(*c*) illustrates that the onset condition for violent dynamic system instability is circumvented as $\frac{\partial C_{\Psi'}}{\partial \phi} < 0$ (Greitzer et al., 2007). Therefore, the RDR is robust, controllable, and inherently free of large-scale system instability (*i.e.,* negative aerodynamic damping) over a wide range of operating states. Of course, local instability may still grow within certain blade rows.

These features are achieved by imparting almost all of the available exergy into the fluid as kinetic energy (KE) using high-turning, supersonic impulse rotor blades (see Fig. 3) rather than pressurising the gas. This KE is then rapidly dissipated, through mixing, into internal energy within the diffuser and vaneless space. This allows very high temperatures to be attained in a fraction of a millisecond without a pressure rise across the stage. For example, a temperature change greater than 300 °C

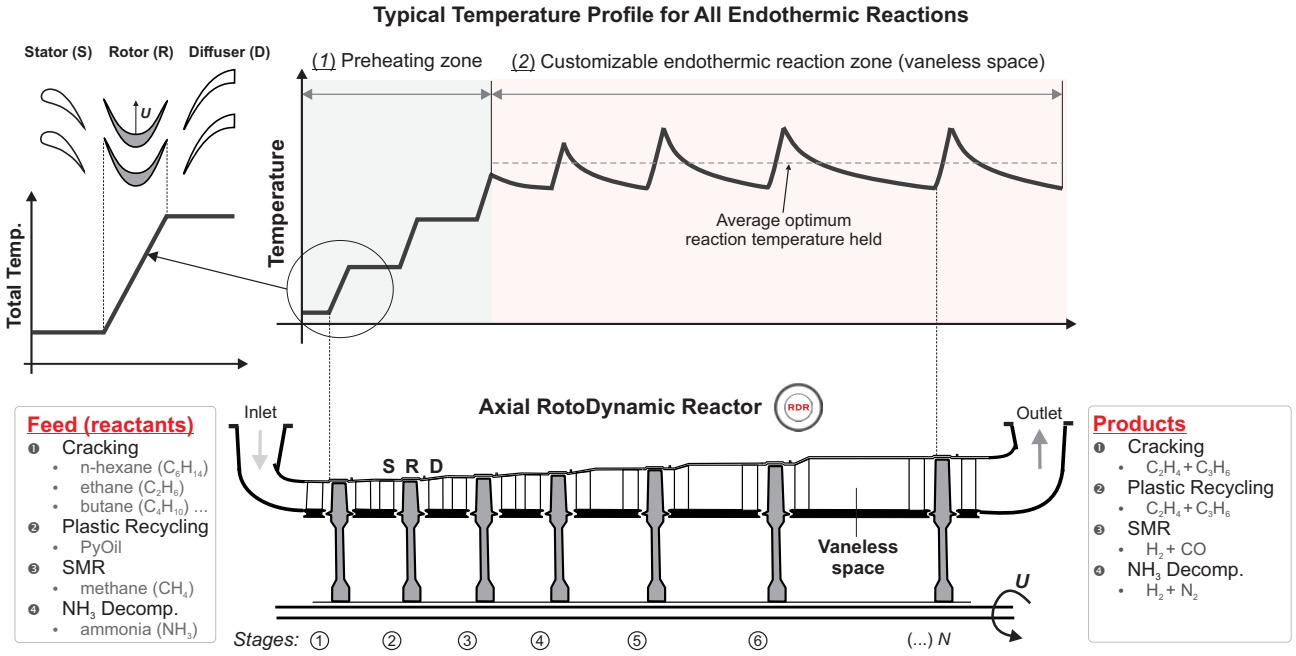

Figure 3 Schematic of the elemental stage and multistage environment for the RotoDynamic Reactor, illustrating a typical total temperature profile for all endothermic chemical processes driven by the RDR

per stage can be achieved with air as the working fluid. As a result, the flow path length required to heat a given mass of fluid to the same temperature can be reduced by nearly two orders of magnitude compared with a furnace (see Fig. 1).

In the multistage environment, the flow must be reconditioned before the next rotor row. A stator vane is used to rapidly accelerate the flow to help it recover before entering the downstream row, as well as provide the necessary high Mach number with a large negative swirl angle (to the rotor). The favourable pressure gradient attenuates residual flow non-uniformities from the upstream mixing process, ensuring high performance across the multistage architecture (Karefyllidis et al., 2023).

Addressing the Limitations of Surface Heat Exchange

Compared to radiant furnaces, the RDR provides a fundamental advantage: mechanical energy is directly transferred into the fluid, making it the hottest part of the system. This is in contrast to furnaces, where the walls are the hottest part of the system due to the heat transfer process. This inherent feature of a turbomachine bypasses two key challenges encountered in radiant coils. First, the heat transfer area requirement is avoided, allowing a significantly shorter gas path (see Fig. 1). Reaction selectivity is a function of residence time; therefore, the primary product yield can be increased.

Second, as indicated in Fig. 1, the thermal and velocity boundary layers within the tubes are thick and mismatched. As a result, the majority of the fluid's mass is concentrated at the centre, but the highest temperature is at the surface. This results in coke deposition on the walls due to high metal temperatures (for hydrocarbon feeds) and overcracking due to nonhomogeneous reaction progress. By avoiding these limitations, the RDR enables a more homogeneous and efficient reaction for all chemical processes, as well as lower coking rates for hydrocarbon-based feeds.

Fine-Tuned Control of the Endothermic Reaction Dynamics

For high-temperature endothermic chemical reactions, where the enthalpy of reaction $\Delta_{rxn}H^0_{298}$ is positive, a turbomachine can be used to replace conventional radiant furnaces. The turbo-reactor preheats the gas mixture to a temperature where the reaction proceeds efficiently, followed by further customised stages to maintain the average temperature during the subsequent enthalpy-draining reaction, as shown in Figure 3. This paper will show the versatility of the RDR is showcased using the four example applications (see Fig. 4) summarised below:

1. Steam cracking: transforming heavy hydrocarbons into higher-value olefins such as ethylene (C_2H_4) and propylene (C_2H_6). This is a thermal decomposition (*i.e.,* pyrolysis) reaction in an oxygen-free environment.

2. Thermochemical recycling of mixed plastic waste (Kusenberg et al., 2022): decomposing pyrolysis oil (PyOil) back into virgin-quality olefins (see Fig. 4). Olefins are created using the same steam cracking process mentioned above.

3. Steam methane reforming: the RDR is used to produce syngas (CO + H_2) from natural gas (CH_4). This syngas is processed and separated into hydrogen (H_2) and carbon dioxide (CO_2) (Rostrup-Nielsen and Christiansen, 2011).

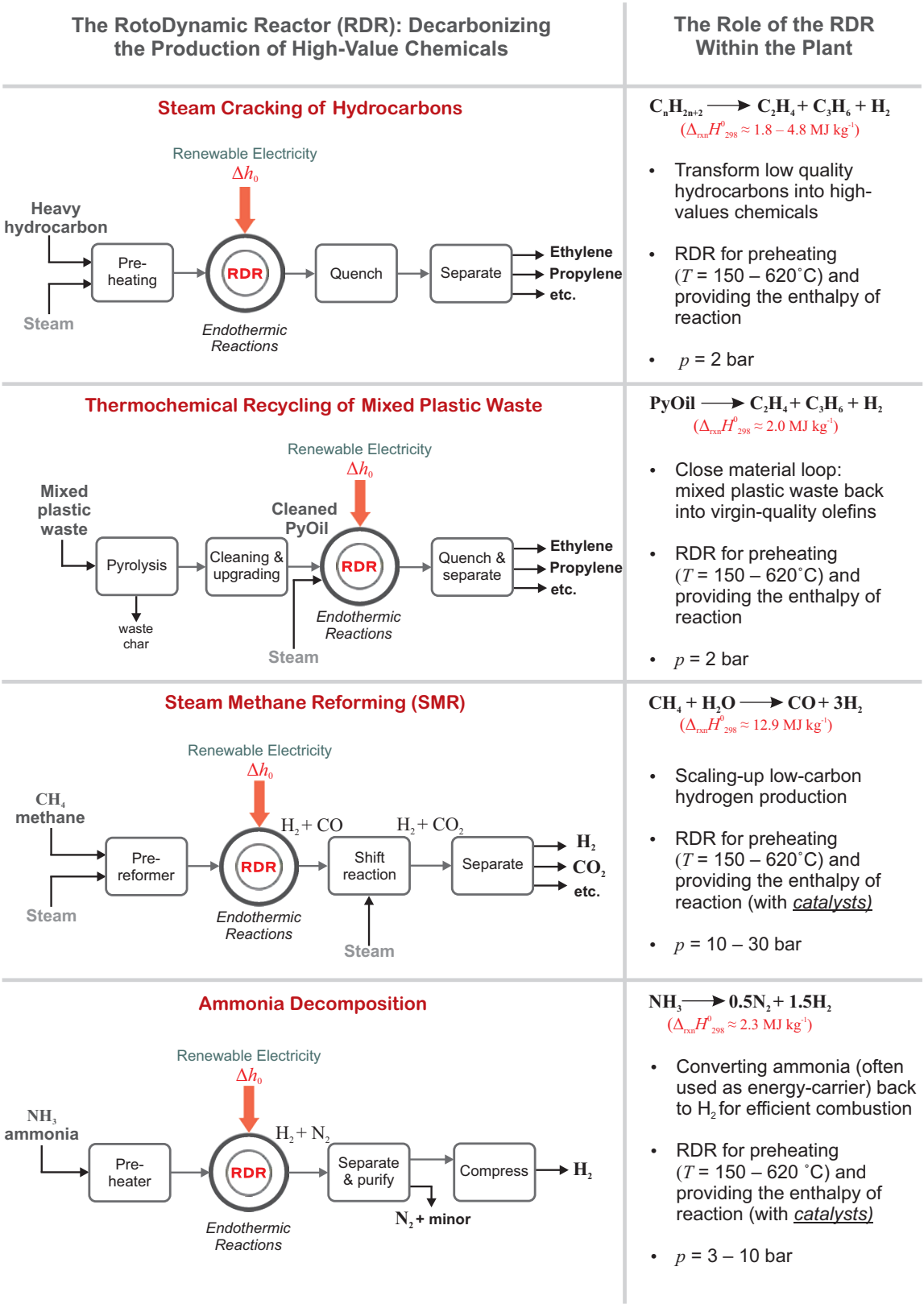

Figure 4 Schematic illustration of potential opportunities for turbomachines to decarbonise high-temperature endothermic reaction processes in the chemical and petrochemical industry

4. Ammonia (NH_3) decomposition: converting ammonia into hydrogen (H_2), which is becoming an important process to release H_2 from an ammonia energy carrier for cleaner and more efficient combustion (Jackson et al., 2019).

A common feature among the working fluids used in these applications is that they are all superheated vapours fol-

lowing the ideal gas law with a temperature-dependent heat capacity (*i.e.,* the mixture is a semi-perfect gas). In the first three applications, superheated steam is added to the feed to reduce the coke (*i.e.,* solid carbon) deposition on the surfaces. Therefore, steam plays a crucial role in determining the properties of the mixture. The fact that the mixture is a single-phase, semi-perfect gas significantly simplifies turbomachinery design and modelling processes.

The objective of the non-reacting, ultra-fast preheating section ($150 \leq T \leq 620$°C) for all chemical processes is to maximise the flow of energy into the fluid within a minimum distance and time scale. In some configurations of the preheating zone, the vaneless space can be eliminated by integrating the diffuser and the stator. As a result, the flow enters successive stages with a higher and higher flow coefficient, enabling an increase in stage loading across the multistage architecture (until an equilibrium is reached).

Once preheating is complete and the gas mixture is at the reaction-activation temperature, the vapour enters the reaction zone where the turbo-reactor provides a tailored temperature profile based on the process-specific reaction dynamics (see Fig. 3). This is achieved using a non-uniform axial distribution for the interstage vaneless space length (see Fig. 3). For each stage, its axial dimension depends on the local heat of reaction, which is a function of the thermochemical state.

NUMERICAL METHODOLOGY

In the following sections, the versatility of the turbo-reactor will be demonstrated in its ability to operate effectively across a wide range of feedstocks and reaction conditions for various chemical processes powered by the RDR. Their basic requirements, based on the design of the datum stage, are summarised in Table 1. To evaluate the performance of the machine under these varying conditions without relying on computationally-intensive reacting flow simulations, a framework has been developed to decouple the aerodynamics and chemical kinetics, which will be introduced in the next section.

Table 1 Approximate preliminary requirements for the preheating and reaction zones based on the datum stage

Feed/Process	Preheating Zone (150°C < T < 900°C)			Reaction Zone ($T \approx$ 900°C)		
	Approx. No. stages	Residence time (ms)	Energy-input (MJ kg^{-1})	Approx. No. stages	Residence time (ms)	Energy-input (MJ kg^{-1})
n-Hexane	8	4.0	2.4	6	11	1.8
Ethane	8	4.0	2.4	13	27	3.9
SMR: methane†	7	3.5	2.1	12 – 18	20 – 250	4.0 – 12.0
Ammonia‡	8	4.0	2.4	12	170	3.6

†with Nickel catalyst* ‡with Ruthenium catalyst* *Surface-area-to-volume ratio = 400 m^{2}m^{-3}

A Decoupled Framework for Evaluating the Effects of Chemistry on Aerothermal Performance

A low-order approach is taken to decouple computational fluid dynamic (CFD) simulations and chemical kinetics. This is summarised in Fig. 5 and can be explained as follows. Offline, 1-D detailed kinetic simulations are conducted for steam cracking (of an n-hexane and ethane feed), SMR, and ammonia decomposition reactions across a broad temperature range ($150\,^{\circ}\text{C} \leq T \leq 1000\,^{\circ}\text{C}$) covering both the preheating and reaction zones. All of the reactions are taken near completion to capture a broad range of reaction states.

The impact of the chemical reaction is effectively lumped into changes in the fluid properties, with four variables forming the parameter space: static temperature T, heat capacity ratio γ, isobaric specific heat capacity c_p and dynamic viscosity μ. By sampling from this fluid property space (see Fig. 5) and performing CFD for each sample, the performance can be evaluated under different reaction conditions without performing costly reacting flow simulations. The aerothermal performance of the turbomachine is characterised in the same way as a conventional turbomachine by four nondimensional groups shown in Eq. 1 and defined in Dixon and Hall (2013):

$$\underbrace{\frac{p_{02}}{p_{01}}}_{\text{Total pressure ratio}},\ \frac{\Delta T_0}{T_{01}},\ \underbrace{\psi}_{\text{Stage loading coeff.}} = f\left(\underbrace{\frac{\dot{m}\sqrt{\gamma R T_{01}}}{D^2 p_{01}}}_{\text{Capacity func.}},\ \underbrace{\frac{\Omega D}{\sqrt{\gamma R T_{01}}}}_{\text{Non-dim. blade speed}},\ \underbrace{Re}_{\text{Reynolds number}},\ \gamma\right) \tag{1}$$

where p_0 is the total pressure, R is the gas constant, $\dot{m}$ is the mass flow rate, D is the mean diameter, and Ω is the rotational

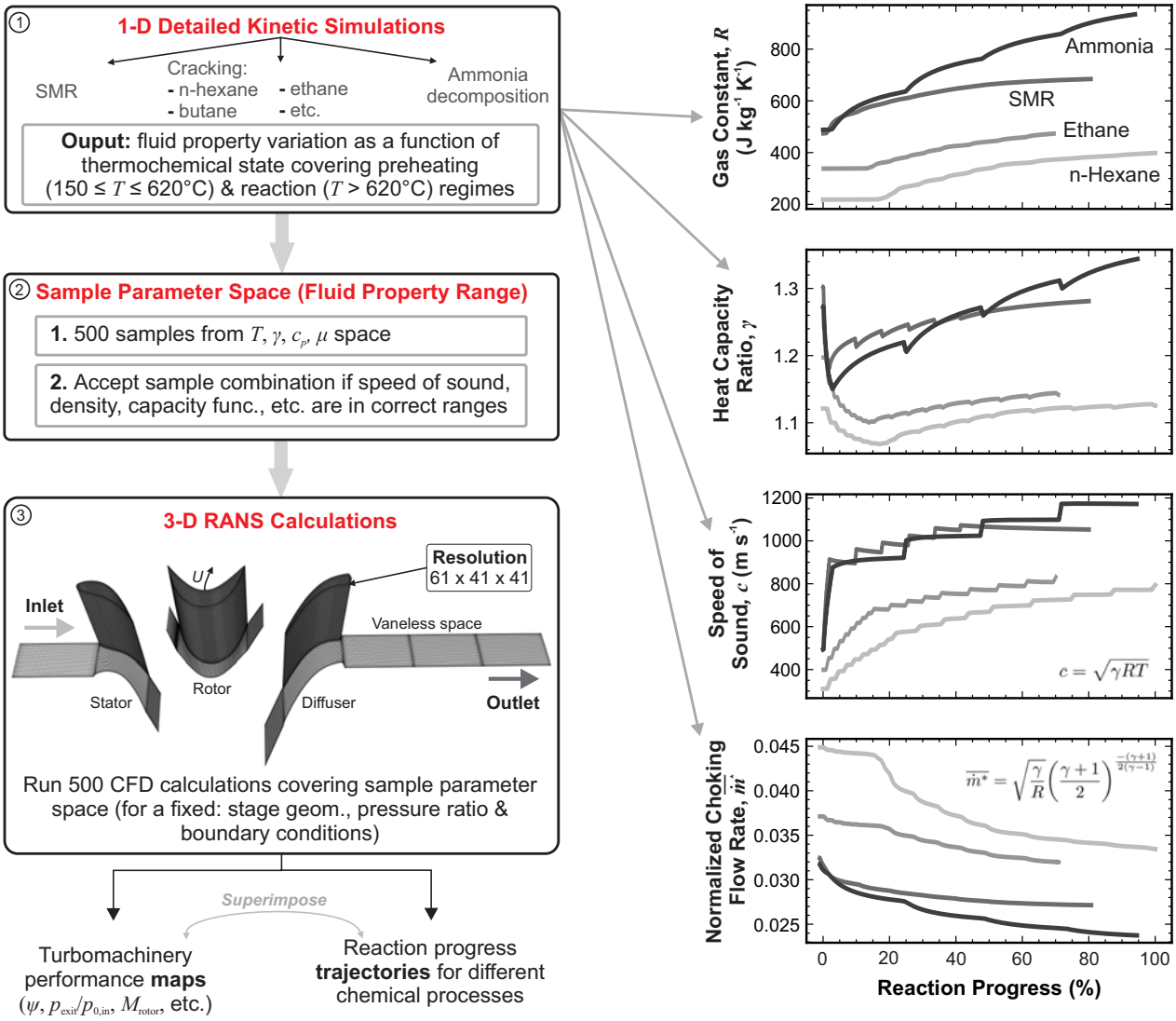

Figure 5 (*Left*) The methodology for constructing performance maps of the RDR for a broad range of chemical processes and reaction states and (*Right*) temperature-dependent variations in thermophysical properties, speed of sound, and non-dimensional choking mass flow rate w.r.t. reaction progress in the range 150 – 1000 °C

speed. The terms highlighted in red are composition dependent, indicating that turbomachinery performance is a direct function of the state of progress through each reaction.

Block (1): 1-D Chemical Kinetic Modelling

For each feedstock and chemical process illustrated in Block (1) of Fig. 5, a chemical reaction mechanism is automatically generated using RMG-Py (Gao et al., 2016). This includes both gas-phase reactions and heterogeneous surface-phase (catalytic) reactions. An in-house 1-D reactor model, built on top of a plug-flow reactor (PFR) model and stiff ordinary differential equation solver within Cantera (Goodwin et al., 2022), is used to approximate the enthalpy supplied by the rotor separated by user-defined time intervals representing the residence time per stage. Both ammonia decomposition and SMR require catalysts. For both, the surface-area-to-volume ratio is set to 400 $m^2\,m^{-3}$, which could be tuned where required.

The validity of the semi-perfect gas assumption for each chemical reaction was further analysed. A real gas equation of state was used to simulate the gas mixtures over the relevant operating points, and for almost all regimes, the compressibility factor Z and fugacity coefficient Φ deviated by less than 2% from their ideal gas values. For SMR, at low temperatures of $T \leq 200\,°C$ and at high pressures of 30 bar, the deviation from ideality increased to a maximum of ≈8% for Z and Φ. However, the error quickly dropped to a negligible level once the temperature rose by 100 °C. This provides confidence in the semi-perfect gas assumption over an extensive range of conditions and feeds.

Block (2): Sampling the Fluid Property Space

The parameter space is formed by randomly sampling from T, γ, c_p, and μ. As the nondimensional groups on the right-hand side of Eq. 1 involve *combinations* of these parameters, such as the stagnation speed of sound $\sqrt{\gamma RT_{01}}$, only random samples of the parameter space that fall within the known range of capacity function, speed of sound, nondimensional blade speed, etc., are accepted. These *known ranges* are determined by precursor 1D chemical kinetic simulations covering a range of feedstocks and feed conversion states (see previous section).

Block (3): 3-D Steady RANS CFD Modelling

To evaluate the aerothermal performance, 500 steady three-dimensional, non-reacting RANS calculations using a single stage were performed for each sample in the parameter space (see Block (3) in Fig. 5). This was achieved using the flow solver Tblock (Denton, 1983, 1986, 1992) with a mixing length turbulence treatment. The mixing length scale is tuned on a block basis based on the turbulent length scale found using high-fidelity LES. The computational setup, which employed a simplified computational domain and numerical treatment, allowed for hundreds of CFD simulations to be run in a short amount of time. To assess mesh independence, three grades of mesh density were simulated. The mass-averaged flow coefficient, stage loading coefficient, and rotor exit Mach number error were within 0.7%, 1.9%, and 2.0%, respectively. This gives us confidence in the trends presented in the following sections.

ROBUSTNESS OF THE TURBO-REACTOR CONCEPT TO FEED VARIABILITY

This paper presents the first instance in turbomachinery in which reactions occur across the full gas path length, resulting in significant variations in the thermophysical fluid properties from inlet to outlet. These changes cover a broad range of molecular weights and have a reaction-dependent impact on turbomachinery performance, specifically on the gas dynamics ($c = \sqrt{\gamma RT}$, γ, $\overline{m^*}$, etc.). In this section, we demonstrate the controllability of the machine over a broad range of Reynolds numbers, Mach numbers, and flow coefficients to illustrate its robustness to feed variability.

Influence of Reynolds Number on Aerodynamic Performance

The Reynolds number $Re = \frac{\rho V_x C_x}{\mu}$ (seen in Eq. 1) varies with feed composition and reaction progress due to changes in fluid density and dynamic viscosity. Figure 6(a) suggests that stage loading is weakly dependent on Reynolds number over a wide range ($1 \times 10^4 \leq Re \leq 2.5 \times 10^6$), dropping by only 9% over the investigated range. As expected, more energy can be imparted into the fluid at high Reynolds numbers. Figure 6(b) indicates that this is because, in the low Reynolds number regime, there is a higher level of separation since the boundary layer is more sensitive and can no longer negotiate local adverse pressure gradients. Despite the higher boundary layer separation, the strong pressure differential between the pressure surface (PS) and the suction surface (SS), typical of impulse blading, overshadows viscous effects. As a result, the impact on the stage loading coefficient is relatively small (see Fig. 6(a)).

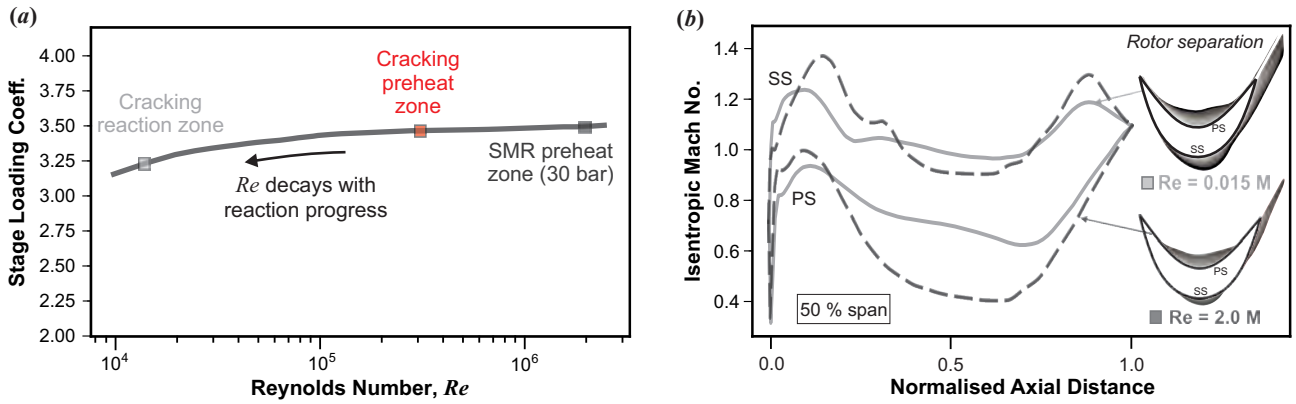

Figure 6 (*a*) Variation of stage loading with Reynolds number ($Re = \frac{\rho V_x C_x}{\mu}$) and (*b*) isentropic Mach number distributions for two extreme Reynolds number states, corresponding to different reactions powered by the RDR

Turbomachinery Performance Maps Covering A Wide Operating Range

This section demonstrates the applicability of using a turbomachine for four different reacting chemical processes using a uniform stage design and fixed boundary conditions. These conditions include a fixed imposed pressure ratio $p_{exit}/p_{0,in} \approx 0.98$ and blade tip speed. As highlighted at the bottom right of Fig. 7, by varying the fluid properties (see Fig. 5) while fixing $p_{exit}/p_{0,in}$, the system naturally experiences variations in the operating point, set by the flow coefficient $\phi = V_x/U$. This variation is exploited in order to probe the response of the dynamical system (*i.e.,* the RDR) subject to input perturbations

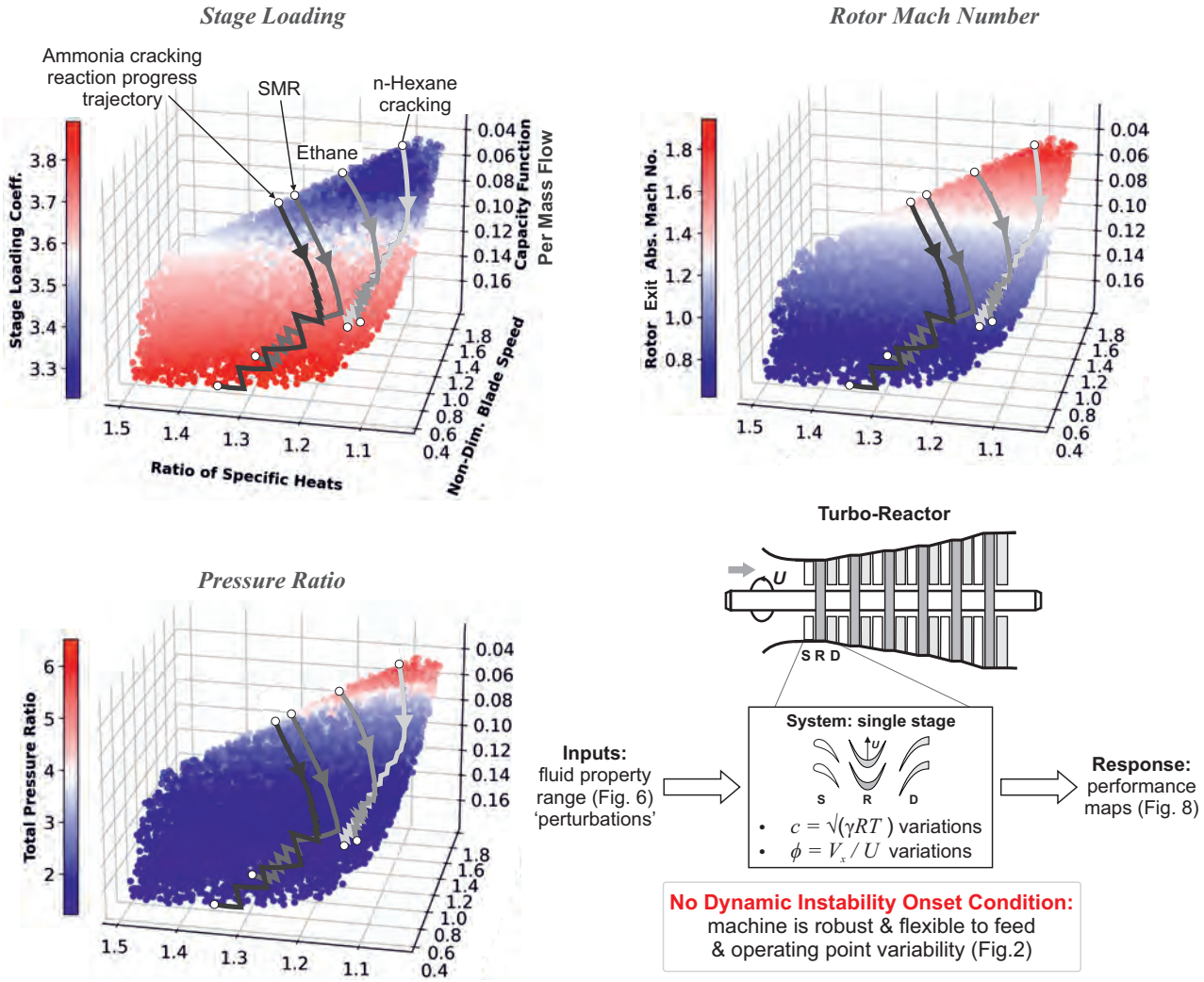

Figure 7 Performance maps showcasing the trajectories of four applications of the turbo-reactor (for a fixed Re = 100,000 and pressure ratio $p_{exit}/p_{0,in}$ = 0.98), presented as a function of reaction progress with thick lines

(*i.e.,* fluid properties). As a result, the robustness and controllability of the machine can be demonstrated on a wide range of fluid properties and operating regimes. Of course, during normal operation, the delivery pressure and stage design can be customised for each reaction and progress state to maintain the optimum velocity triangles.

Each thick solid line indicated in Fig. 7 represents the trajectory through the evolution of a reaction calculated using detailed 1-D kinetic calculations. This detailed chemical analysis is done independently and the results are superimposed on the performance maps. These thick lines effectively illustrate how the aerothermal performance varies in the streamwise direction across a multistage machine for each chemical process. For all reactions, the imposed pressure ratio is fixed; therefore, the Mach number decays across the multistage machine through the reaction evolution. Since density decreases, this is accompanied by an increase in flow coefficient towards the rear of the machine, enabling a higher stage loading near reaction completion. At the beginning of the reaction, the feeds are initially separated in the non-dimensional parameter space (see Fig. 7). However, as the reactions progress, they all converge towards the higher-loading region.

More generally, two insights can be gained from the response of the performance metrics shown in Fig. 7. First, the ratio of specific heats has a relatively small impact on the stage loading. Secondly, the dominant parameters driving changes in flow physics are the non-dimensional blade speed and flow coefficient. The non-dimensional blade speed is inversely proportional to the speed of sound (see Fig. 5 and Eq. 1) and varies by almost a factor of 4.5, whilst the flow coefficient, which sets the velocity triangles, varies by almost a factor of 2 (due to the density variation). The stage loading coefficient does not respond significantly, with a maximum deviation of only 15%, illustrating the robustness of the turbo-reactor despite using a fixed elemental stage. This margin can be further reduced by adjusting the delivery pressure to restore the velocity triangles. Since there is no onset condition for violent system instability (see Fig. 2(*c*)), the machine can provide a high enthalpy input over a broad range of reaction and operating states.

Parameter Space Boundaries: Extremes of the Mach Number Regime

Two extreme Mach number regimes, covering a wide range of feed molecular weights (1.0 – 86.0 $\mathrm{g\,mol^{-1}}$) and hence the speed of sounds (280 – 1150 $\mathrm{m\,s^{-1}}$), are selected from the parameter space shown in Fig. 7 and are compared in more detail in Fig. 8. The low Mach number regime corresponds to an ammonia feed toward reaction completion, and the high Mach number regime corresponds to an n-hexane feed before the reaction starts. The first case represents a front stage of the machine, which is capacity-limiting due to the low speed of sound (see Fig. 5 (*Right*)), and the second case represents a rear stage. The high Mach number case (see Fig. 8 (*Right*)) is presented to illustrate the robustness of the flow at off-design regimes. However, in practice, the mismatched velocity triangles can be partially corrected by adjusting the delivery pressure to accommodate a higher mass flow rate. However, since the flow is close to a fully choked state, the level of control available is limited. Therefore, the designer must resort to modifying the stage design to improve the swallowing capacity and specific energy input rate. For example, the blade count could be reduced or the annulus area increased in order to increase the throat area, thus improving the throughflow capacity.

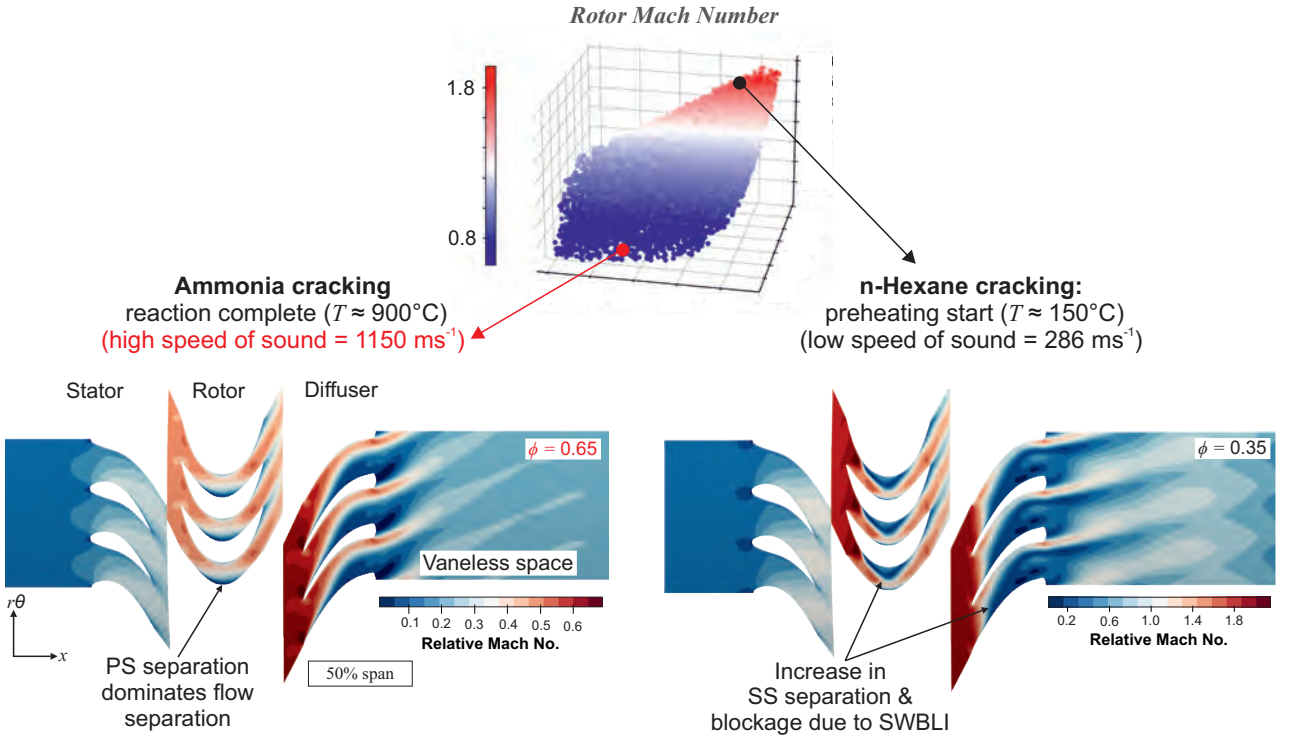

Figure 8 Comparison of the midspan relative Mach number distribution at two 'extreme' corners of the parameter space where fluid properties and local gas composition lead to two polar speed of sound regimes

Fig. 8 provides three key insights into the flow physics of the system. First, within the rotor, the low Mach number case is mainly affected by PS separation and blockage, whereas for the high Mach number case, an increased positive incidence angle results in a higher level of SS separation contaminating the flowfield. This is because (I) the flow coefficient drops by almost a factor of 2 for the high Mach number case (II) the Mach number is supersonic, making the flow sensitive to small changes in incidence ($\leq 1.5°$), and (III) a shockwave at the rotor inlet contributes to further SS boundary layer separation through shockwave boundary layer interaction (SWBLI).

Secondly, the gas mixture in the low Mach number regime (Fig. 8 (*Left*)) consists of 70% hydrogen on a mole basis. As hydrogen has a low molecular weight and hence a high speed of sound, it can accommodate a higher flow coefficient at a given pressure ratio. This allows for a greater change in tangential velocity whilst avoiding the SWBLI in the rotor, resulting in higher stage loading (see Fig. 8). As the flow is far below the choking limit, an even higher flow coefficient can be attained by increasing the delivery pressure (see Fig. 2(*b*)). Thus, the local fluid properties (set by the local composition state) have a significant influence on the operating range, compressibility, and loading capabilities for a fixed geometry. With the current datum design, the operating range of the high molecular weight n-hexane feed (Fig. 8 (*Right*)) is more restricted, and the ϕ–ψ characteristic is almost vertical (see the low speed of sound boundary in Figs 2(*b*) & (*c*)). However, for a given fluid, the design can be altered to balance the operating range and the specific energy input rate per stage.

Finally, the results presented demonstrate that the RDR can still achieve a reasonably high level of specific energy input ($\Delta h_0 = 220\,\mathrm{kJ\,kg^{-1}}$) despite large-scale flow separation due to incidence and SWBLI, as indicated in Fig. 8 (*Right*). This flexibility of the machine is a direct consequence of isentropic efficiency not impacting the performance of the machine.

Without a requirement to resist an adverse pressure gradient, entropy can be generated without dramatic repercussions for the specific energy that can be imparted into the fluid. Despite an elevated level of flow separation within the passage, the flow within the rotor is turned through an angle close to the blade metal angles. Therefore, the specific energy imparted into the fluid remains high, albeit at the expense of a reduced flow coefficient due to blockage. In the high Mach number regime, a higher total pressure ratio across the rotor (see Fig. 7) results in an increased local choking mass flow rate. This ensures that a reasonable level of mass can still be swallowed, despite the reduction in the effective throat area due to blockage in the diffuser. As the total pressure is quickly dissipated downstream, there is no global adverse pressure gradient (see next section). It is noted that the blockage varies radially; for example, toward the tip, the incidence angle and area ratio are such that the flow remains more attached within the passage and a greater flow rate can be passed locally.

A Breakdown of the Energy Conversion Mechanisms

Once kinetic energy (KE) has been absorbed by the flow through the rotor, it must eventually be dissipated into internal energy u within the diffuser and vaneless space. In some configurations of the machine, such as the ultra-fast gas preheating zone before the reaction starts, the vaneless space can be removed, and the majority of the energy dissipation occurs every 2 – 4 stages. In contrast, for a gas mixture undergoing reactions, it is more optimal to dissipate the mechanical energy at every stage to repeatedly balance and compensate for the drop in temperature caused by the reaction.

A well-designed energy transformation system aims to convert kinetic energy into internal energy over the minimum possible time scale, typically less than 0.5 ms. This is achieved controllably through both an isentropic diffusion mechanism, as well as through entropic dissipation mechanisms equivalent to aerodynamic losses. By exploiting entropic dissipation ds, the static temperature rise dT can be maximised within a minimum time scale while killing any minor unwanted static pressure gains dp. This principle can be expressed by the Gibbs equation $c_p dT = \frac{1}{\rho} dp + T ds$. Exploiting aerodynamic losses in this way is in stark contrast to conventional energy-imparting machines.

Figure 9 illustrates the quantitative breakdown of energy conversion mechanisms at the two flow regimes shown in Fig. 8 above. Other conversion sources, such as leakage, are neglected. The energy conversion breakdown is determined by integrating the viscous dissipation share $\dot{S}_{\text{vsic}}$ of the total entropy generation rate (Denton, 1993) zonally for five regions in the diffuser-vaneless-space system listed in Fig. 9 (*Left*). A more detailed description of the 'loss audit' methodology can be found in Pullan et al. (2004); Moore and Moore (1983). The sixth energy conversion mechanism accounted for is isentropic diffusion $\zeta_{\text{isentropic}}$, which is calculated using isentropic relations between two known states. Equation 2 is used to calculate the the entropic portion ζ_{entropic} of the total energy conversion coefficient $\zeta = \zeta_{\text{isentropic}} + \zeta_{\text{entropic}}$.

$$\zeta_{\text{entropic}} = \frac{\dot{S}_{\text{vsic}} T_{\text{exit}}}{\dot{m} \Delta h_{0,\text{rotor}}}, \quad \text{where} \quad \dot{S}_{\text{visc}} = \iiint_{V'} \frac{1}{T} \tau_{ij} \frac{dV_i}{dx_j} dV' \tag{2}$$

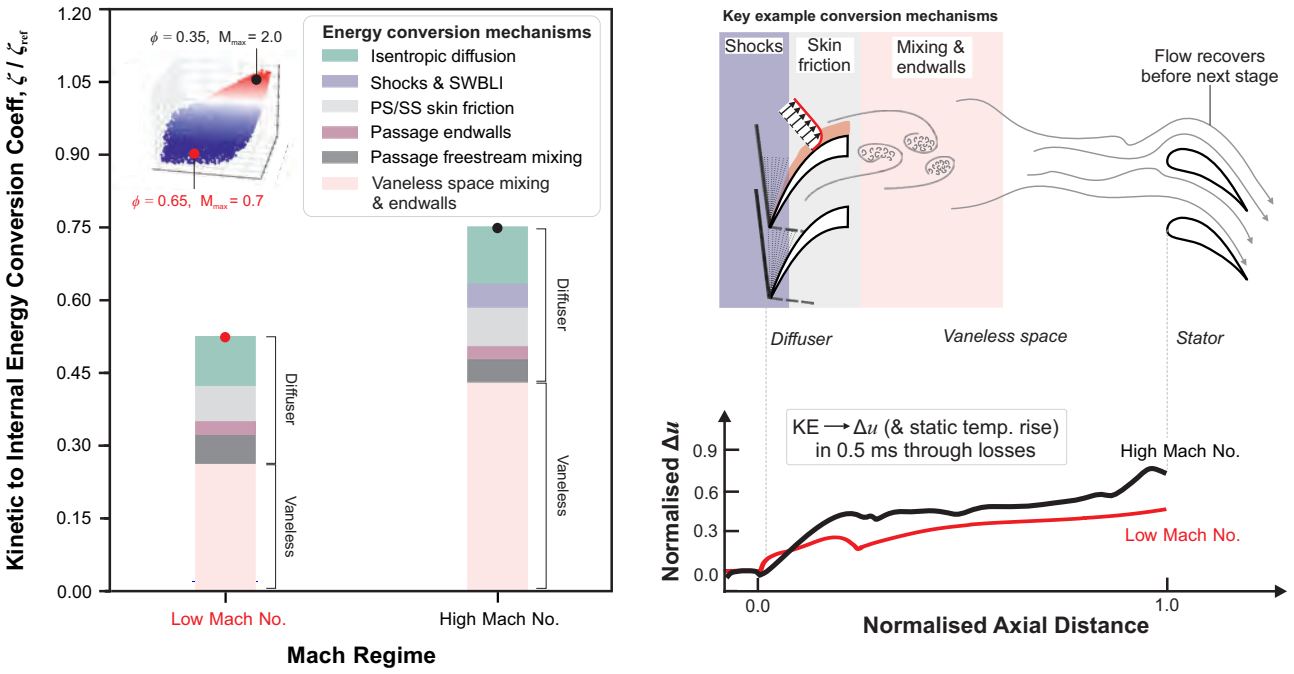

Figure 9 A breakdown of kinetic energy (KE) to internal energy ($\Delta u = c_v \Delta T$) conversion mechanisms including both entropic dissipation and isentropic diffusion sources. The breakdown for a single stage is compared for two extreme Mach regimes corresponding to thermophysical properties encountered in two different chemical processes

Figure 9 illustrates redistribution between the energy conversion mechanisms for the two feeds at different reaction states. In the low Mach number regime (*i.e.,* high-temperature decomposed ammonia), boundary layer viscous dissipation dominates within the blade passage since the velocities at the boundary layer edge V_δ are high and scale as V_δ^3 (Denton, 1993). The entropy generated within the boundary layer is convected and diffused downstream. For both cases, there is a 15 – 20% contribution to energy conversion due to reversible, isentropic diffusion as the flow area expands. The contribution for the high Mach number regime (*i.e.,* low-temperature n-hexane) is greater as the static pressure ratio across the diffuser-vaneless-space system is higher. Additional isentropic static pressure and temperature rise are provided by discontinuous changes in properties through the shockwave. This is lumped into the isentropic diffusion subcategory.

Vortex shedding generated by a thick trailing edge (approximately 30% of the blade pitch), coupled with a sudden expansion of the flow downstream of the diffuser, leads to significant mixing losses. As a result, 50 – 65% of energy conversion occurs within the vaneless space. In the high Mach number regime, there is a high level of energy conversion in the vaneless space as the trailing edge mixing loss is a function of Mach number Denton and Xu (1990).

In the high Mach number regime, there is an additional 'shock' energy conversion mechanism. Additional loss due to shock-induced separation is also lumped into the 'shock' category shown in light purple in Fig. 9. Shock-induced temperature rise and shock-induced flow separation play important roles in the energy transformation process, enabling a higher increase in internal energy compared with the first case (see Fig. 9). The temperature ratio across the shock scales with pre-shock Mach number normal to the shock $T_2/T_1 \propto M_n^2$. Since the oblique shock angle is relatively shallow at midspan, the normal component of the Mach number is low, indicating that the effect of shock-induced separation dominates over shock-induced temperature rise. However, towards the blade tip, there is a change in incidence that leads to a more intense shock system within the passage, along with shocks in the vaneless space. This results in a spanwise nonuniformity in the distribution of energy conversion from hub to tip.

This analysis shows that despite variations in the incoming dynamic head over a wide range of operating points and feeds, the dissipation of kinetic energy into internal energy to obtain the required temperature rise can still be achieved over a short distance. The flow naturally redistributes the processing mechanisms to ensure sufficient dissipation depending on the level of incoming kinetic energy, the Mach regime, and the flow state. In other words, the flow self-adjusts the contributions from each conversion mechanism to match the downstream boundary condition. However, if kinetic energy dissipation is insufficient for certain flow regimes, aerodynamic devices can be introduced to enhance the rate of heat generation.

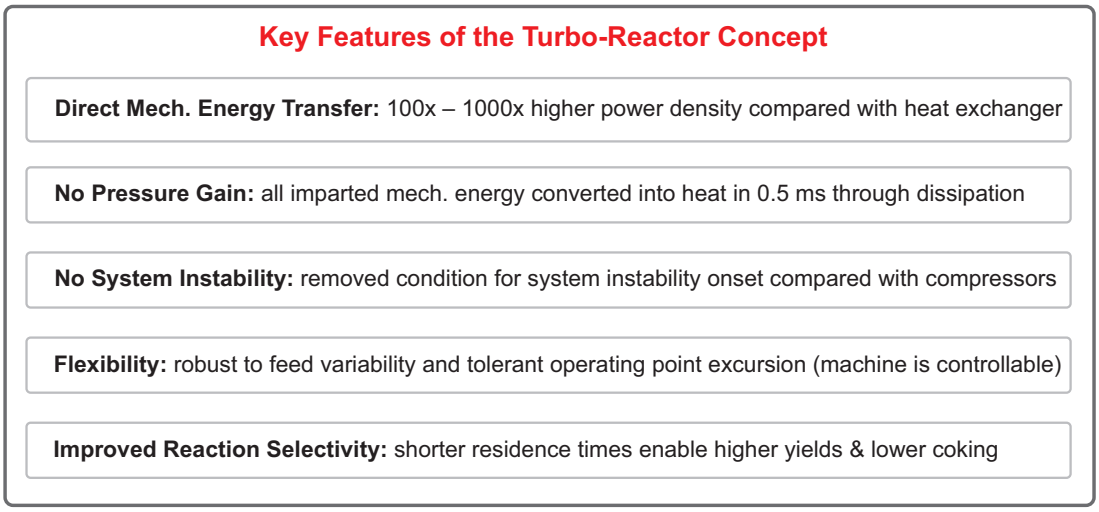

Figure 10 Schematic block diagram summarising the key features of the new RDR concept

SUMMARY AND CONCLUSIONS

This study has demonstrated the feasibility of using an electric-motor-driven turbomachine to mitigate carbon emissions and improve the operability, controllability, and reaction performance of four crucial energy-intensive, endothermic reaction processes. The numerical investigation presented in this paper has revealed several key design characteristics of the concept summarised in Fig. 10, which are as follows:

1. The RDR is shown to operate effectively over a range of feeds and reaction states using a uniform design. Since the collection of molecular weights covered is extensive, other relevant chemical processes should fall within this range.

2. The controllability of the turbomachine has been successfully demonstrated over a wide range of operating and Mach number regimes by inducing operating point excursions through fluid property perturbations. The stage loading

only dropped by 15% over a broad set of flow conditions, indicating the robustness of the RDR. Additionally, the turbomachine showed a weak Reynolds number dependence, with only a 9% variation over two orders of magnitude of the Reynolds number.

3. Without a requirement for pressure gain, the design restrictions of efficiency and system instability are no longer relevant. Therefore, a high level of incidence and separation can be endured, facilitating a high level of energy input and swallowing capacity over the operating range. The limits of the RDR are set only by choking (which is a restriction on the throughflow capacity of the machine) and not system instability.

4. Over a broad range of gas velocities and Mach numbers—corresponding to different feeds and reaction states—this work has shown that kinetic energy can be dissipated into internal energy (and static temperature rise) over an extremely short time scale of 0.5 ms, enabling a compact machine for ultra-fast gas heating. The breakdown of conversion naturally self-corrects to ensure sufficient transformation of the incoming dynamic head at different Mach and velocity regimes.

In summary, a turbomachine is a robust and efficient means of heating a wide variety of (endothermically) *reacting* gas mixtures to high temperatures. This analysis covers a broad spectrum of fluid properties, therefore suggesting that a similar elemental stage design could also be used to heat other *non-reacting* gas mixtures, enabling decarbonisation of energy-intensive industries, such as steel, cement, glass, and aluminium, whilst simultaneously reducing the footprint of the plant 100 – 1000×.

NOMENCLATURE

Symbols

$c = \sqrt{\gamma RT}$	speed of sound, $\mathrm{m\,s^{-1}}$
$C_{\Psi'} = \frac{p_{\text{exit}} - p_{0,\text{in}}}{p_{0,\text{in}}}$	total-to-static pressure rise coefficient
c_p	isobaric heat capacity, $\mathrm{J\,kg^{-1}\,K^{-1}}$
c_v	isochoric heat capacity, $\mathrm{J\,kg^{-1}\,K^{-1}}$
C_x	axial chord length, m
h_0	stagnation enthalpy, $\mathrm{J\,kg^{-1}}$
$\Delta_{\text{rxn}}H^0_{298}$	enthalpy of reaction, $\mathrm{J\,kg^{-1}}$
$\overline{m^*}$	non-dimensional choking mass flow rate
p	static pressure, Pa
p_0	stagnation pressure, Pa
R	gas constant, $\mathrm{J\,kg^{-1}\,K^{-1}}$
$Re = \frac{\rho V C_x}{\mu}$	Reynolds number
$\dot{S}_{\text{vsic}}$	viscous entropy generation rate, $\mathrm{W\,K^{-1}}$
T	static temperature, K
Δu	internal energy change, $\mathrm{J\,kg^{-1}}$
U	mean blade speed, $\mathrm{m\,s^{-1}}$
V'	domain volume, $\mathrm{m^3}$
V_x	axial velocity, $\mathrm{m\,s^{-1}}$
$\gamma = \frac{c_p}{c_v}$	heat capacity ratio
ζ	energy conversion coefficient
μ	dynamic viscosity, Pa s
$\psi = \frac{\Delta h_0}{U^2}$	stage loading/work coefficient
$\phi = \frac{V_x}{U}$	flow coefficient
τ_{ij}	shear stress tensor, Pa

Acronyms

PFR	plug-flow reactor
PS/SS	pressure/suction surface
RDR	RotoDynamic Reactor (turbo-reactor)
SMR	steam methane reforming
SWBLI	shockwave boundary layer interaction

ACKNOWLEDGEMENTS

The authors would like to thank Coolbrook Oy for supporting this work. The authors are grateful for fruitful discussions with Tuomas Ouni at Coolbrook Oy.

REFERENCES

Bender, M. (2014), 'An overview of industrial processes for the production of olefins–C4 hydrocarbons', *ChemBioEng Reviews* **1**(4), 136–147.

Bushuev, V. A. (2016), 'Bladed reactor for the pyrolysis of hydrocarbons '. *U.S. Patent Application No. US 9.494,038 B2*. Washington, DC: U.S. Patent and Trademark Office.

Coolbrook Oy (2022), Coolbrook Oy. Helsinki, Finland, accessed Oct. 15, 2022, https://coolbrook.com.

Delikonstantis, E., Scapinello, M. and Stefanidis, G. D. (2019), 'Process modeling and evaluation of plasma-assisted ethylene production from methane', *Processes* **7**(2), 68.

Denton, J. D. (1983), 'An Improved Time-Marching Method for Turbomachinery Flow Calculation', *ASME. J. Eng. Power* **105**(3), 514–521.
URL: *https://doi.org/10.1115/1.3227444*

Denton, J. D. (1986), The Use of a Distributed Body Force to Simulate Viscous Effects in 3D Flow Calculations, Vol. Volume 1: Turbomachinery of *Turbo Expo: Power for Land, Sea, and Air*. V001T01A058.
URL: *https://doi.org/10.1115/86-GT-144*

Denton, J. D. (1992), 'The calculation of three-dimensional viscous flow through multistage turbomachines', *ASME. J. Turbomach. January* **114**(1), 18–26.

Denton, J. D. (1993), 'The 1993 IGTI Scholar Lecture: Loss Mechanisms in Turbomachines', *Journal of Turbomachinery* **115**(4), 621–656.
URL: *https://doi.org/10.1115/1.2929299*

Denton, J. D. and Xu, L. (1990), 'The Trailing Edge Loss of Transonic Turbine Blades', *Journal of Turbomachinery* **112**(2), 277–285.
URL: *https://doi.org/10.1115/1.2927648*

Dixon, S. L. and Hall, C. (2013), *Fluid mechanics and thermodynamics of turbomachinery*, Butterworth-Heinemann.

Gao, C. W., Allen, J. W., Green, W. H. and West, R. H. (2016), 'Reaction mechanism generator: Automatic construction of chemical kinetic mechanisms', *Computer Physics Communications* **203**, 212–225.

Goodwin, D. G., Moffat, H. K., Schoegl, I., Speth, R. L. and Weber, B. W. (2022), 'Cantera: An object-oriented software toolkit for chemical kinetics, thermodynamics, and transport processes', https://www.cantera.org. Version 2.6.0.

Greitzer, E. M., Tan, C. S. and Graf, M. B. (2007), 'Internal flow: concepts and applications'.

IEA (2021), Global energy review 2021, Technical report, International Energy Agency (IEA).

IEA (2022), Hydrogen, Paris, Technical report, International Energy Agency (IEA).

Jackson, C., Fothergill, K., Gray, P., Haroon, F., Makhloufi, C., Kezibri, N., Davey, A., LHote, O., Zarea, M., Davenne, T. et al. (2019), 'Ammonia to green hydrogen project: Feasibility study', *Ecuity, UK* .

Karefyllidis, N., Rubini, D., Rosic, B., Xu, L. and Purola, V.-M. (2023), A novel axial energy-imparting turbomachine for high-enthalpy gas heating: Robustness of the aerodynamic design, *in* 'Turbo Expo: Power for Land, Sea, and Air', American Society of Mechanical Engineers, p. Accepted Manuscript.

Kusenberg, M., Zayoud, A., Roosen, M., Thi, H. D., Abbas-Abadi, M. S., Eschenbacher, A., Kresovic, U., De Meester, S. and Van Geem, K. M. (2022), 'A comprehensive experimental investigation of plastic waste pyrolysis oil quality and its dependence on the plastic waste composition', *Fuel Processing Technology* **227**, 107090.

Lu, Q., Zhang, B., Yang, S. and Peng, Z. (2022), 'Life cycle assessment on energy efficiency of hydrogen fuel cell vehicle in china', *Energy* **257**, 124731.

Moore, J. and Moore, J. G. (1983), Entropy Production Rates From Viscous Flow Calculations: Part I — A Turbulent Boundary Layer Flow, Vol. Volume 1: Turbomachinery of *Turbo Expo: Power for Land, Sea, and Air*, p. V001T01A032.
URL: *https://doi.org/10.1115/83-GT-70*

Pullan, G., Denton, J. and Curtis, E. (2004), 'Improving the Performance of a Turbine With Low Aspect Ratio Stators by Aft-Loading', *Journal of Turbomachinery* **128**(3), 492–499.
URL: *https://doi.org/10.1115/1.2182000*

Rostrup-Nielsen, J. and Christiansen, L. J. (2011), *Concepts in syngas manufacture*, Vol. 10, World Scientific.

Rubini, D., Karefyllidis, N., Xu, L., Rosic, B. and Johannesdahl, H. (2022*a*), 'A New Robust Regenerative Turbo-reactor Concept for Clean Hydrocarbon Cracking', *Global Power and Propulsion Society* .

Rubini, D., Karefyllidis, N., Xu, L., Rosic, B. and Johannesdahl, H. (2022*b*), Accelerating the development of a new turbomachinery concept in an environment with limited resources and experimental data: Challenges, *in* 'Turbo Expo: Power for Land, Sea, and Air', Vol. 86120, American Society of Mechanical Engineers, p. V10DT36A001.

Rubini, D., Xu, L., Rosic, B. and Johannesdahl, H. (2021), 'A New Turbomachine for Clean and Sustainable Hydrocarbon Cracking', *ASME. J. Eng. Gas Turbines Power* **144**(2). 021024.
URL: *https://doi.org/10.1115/1.4052784*

Thiel, G. P. and Stark, A. K. (2021), 'To decarbonize industry, we must decarbonize heat', *Joule* **5**(3), 531–550.

Venkataraman, K., Wanat, E. and Schmidt, L. (2003), 'Steam reforming of methane and water-gas shift in catalytic wall reactors', *AIChE Journal* **49**(5), 1277–1284.

Weydahl, T., Jamaluddin, J., Seljeskog, M. and Anantharaman, R. (2013), 'Pursuing the pre-combustion ccs route in oil refineries–the impact on fired heaters', *Applied energy* **102**, 833–839.